Published in final edited form as:
Clin Cancer Res. 2010 December 1; 16(23): 5712–5721. doi:10.1158/1078-0432.CCR-10-2055.

Noninvasive Radiofrequency Field Destruction of Pancreatic Adenocarcinoma Xenografts Treated with Targeted Gold Nanoparticles

Evan S. Glazer[1], **Cihui Zhu**[1], **Katheryn L. Massey**[1], **C. Shea Thompson**[3], **Warna D. Kaluarachchi**[1], **Amir N. Hamir**[2], and **Steven A. Curley**[1,4,*]

Evan S. Glazer: eglazer@mdanderson.org; Cihui Zhu: cizhu@mdanderson.org; Katheryn L. Massey: kmassey@mdanderson.org; C. Shea Thompson: ct4@rice.edu; Warna D. Kaluarachchi: wdkaluarachchi@mdanderson.org; Amir N. Hamir: ahamir@mdanderson.org

[1] Department of Surgical Oncology, University of Texas M. D. Anderson Cancer Center, Houston, TX

[2] Department of Veterinary Medicine and Surgery, University of Texas M. D. Anderson Cancer Center, Houston, TX

[3] Department of Biomedical Engineering, Rice University, Houston, TX

[4] Department of Mechanical Engineering and Materials Science, Rice University, Houston, TX

Abstract

Purpose—Pancreatic carcinoma is one of the deadliest cancers with few effective treatments. Gold nanoparticles (AuNPs) are potentially therapeutic because of the safety demonstrated thus far and their physio-chemical characteristics. We utilized the astounding heating rates of AuNPs in nonionizing radiofrequency (RF) radiation to investigate human pancreatic xenograft destruction in a murine model.

Experimental Design—Weekly, Panc-1 and Capan-1 human pancreatic carcinoma xenografts in immunocompromised mice were exposed to an RF field 36 hours after treatment (intraperitoneal) with cetuximab or PAM4 antibody conjugated AuNPs, respectively. Tumor sizes were measured weekly while necrosis and cleaved caspase-3 were investigated with H&E staining and immunofluorescence, respectively. In addition, AuNP internalization and cytotoxicity were investigated *in vitro* with confocal microscopy and flow cytometry, respectively.

Results—Panc-1 cells demonstrated increased apoptosis with decreased viability after treatment with cetuximab conjugated AuNPs and RF field exposure ($p = 0.00005$). Differences in xenograft volumes were observed within 2 weeks of initiating therapy. Cetuximab-conjugated and PAM4-conjugated AuNPs demonstrated RF field-induced destruction of Panc-1 and Capan-1 pancreatic carcinoma xenografts after six weeks of weekly treatment ($p = 0.004$ and $p = 0.035$, respectively). There was no evidence of injury to murine organs. Cleaved caspase-3 and necrosis were both increased in treated tumors.

Conclusions—This study demonstrates a potentially novel cancer therapy by non-invasively inducing intracellular hyperthermia with targeted AuNPs in an RF field. While the therapy is dependent on the specificity of the targeting antibody, normal tissues were without toxicity despite systemic therapy and whole body RF field exposure.

[*]Corresponding author: Steven A. Curley, M.D., 1400 Holcombe Blvd, Unit 444, Houston, TX 77030, scurley@mdanderson.org, Phone: 713-794-4957, Fax: 713-745-5235.

Keywords

gold nanoparticle; radiofrequency field therapy; hyperthermia; cancer; nanotechnology

Despite decades of research in the biology and treatment of pancreatic carcinoma, it remains one of the deadliest and least curable forms of cancer (1,2). Targeted therapy against antigens overexpressed in pancreatic cancer, such as epidermal growth factor receptor (EGFR-1), has only been minimally successful despite its use in other antigen over expressing cancers (3). Clearly, novel therapeutic approaches to treat this disease which kills over 95% of diagnosed patients is needed (4).

Previous reports have demonstrated that metal nanoparticles induce hyperthermic cytotoxicity *in vitro* by exposing the nanoparticles to one of a few forms of nonionizing radiation, specifically near-infrared (NIR) and radiofrequency (RF) (5–8). Furthermore, tumor necrosis has been demonstrated by directly injecting nanoparticles into rodent and rabbit syngeneic cancer implants that subsequently underwent noninvasive RF field exposure(9,10). Importantly, normal tissues tolerate hyperthermia at higher temperatures and for longer periods of time than malignant tissues portending an opportunistic thermal cancer treatment(11).

The previous experimental models suffer from multiple challenges. First, NIR radiation does not penetrate deeply into tissue, limiting its use to superficial malignancies (12–14). Second, if a direct intratumoral injection of nanoparticles is required, then it would necessitate that the tumor be visualized on traditional imaging and require an invasive procedure to actually inject the nanoparticles. Furthermore, direct injection is problematic because nanoparticles will diffuse through malignant and surrounding normal tissue increasing the likelihood of damage to normal cells. Multiple nanoparticles (6,8,15) such as gold, silver, and semiconducting nanoparticles are candidates for hyperthermic treatment, but gold has the most immediate potential for use in human patients and seems to have a favorable safety profile (5,16,17).

Based on previous *in vitro* work (8), we hypothesized that systemic delivery of antibody targeted gold nanoparticles (AuNPs) would induce hyperthermic cytotoxicity after RF field exposure in human pancreatic carcinoma xenografts without injury to normal tissues. Antibodies to 2 distinct human antigens (EGFR-1 and MUC-1) were utilized to deliver 2 different sized AuNPs to 2 unique human pancreatic xenografts. Although EGFR-1 is a problematic therapeutic target due to its diverse constitutive expression in normal tissues, PAM4 is a human antibody to MUC-1 that is specific to pancreatic carcinoma (18). The components were chosen such that the constructs had similar sizes that could lead to increased tumor internalization rates (19). The primary aim was to demonstrate human pancreatic cancer xenograft destruction.

Materials and Methods

Cell culture, antibodies, fluorophores, and gold nanoparticles

Two human pancreatic carcinoma cell lines, Panc-1 and Capan-1, were acquired from the American Type Culture Collection (Manassas, VA), confirmed by the Characterized Cell Line Core Service (M. D. Anderson Cancer Center, Houston, TX, December 2009), and maintained according to ATCC's cell media recommendations in standard conditions (37°C, 5% CO_2). All experiments utilized standard cell culture coated dishes and equipment (BD Biosciences, Franklin Lakes, NJ, Corning Inc., Corning, NY). Cetuximab (C225, Bristol-Myers Squibb, New York, NY), a chimeric monoclonal IgG_1 antibody against human

EGFR-1 was conjugated to 10 nm spherical gold nanoparticles (Ted Pella, Inc., Redding, CA) via a linker. PAM4 (Immunomedics, Inc., Morris Plain, NJ), a human monoclonal antibody against a mucin glycoprotein, MUC-1, was directly conjugated to 20 nm AuNPs (Ted Pella, Inc., Redding, CA) via a thiol-gold bond described below. All fluorophore or fluorophore conjugates were used as directed by the manufacturer (Invitrogen Corp., Carlsbad, CA).

AuNP constructs and characterization

C225 was conjugated via covalent hydrazide-thiol heterobifunctional linker (Sensopath Technologies, Inc., Bozeman, MT) from a previously published protocol with slight modifications based on glycosolation of the Fc region (20). Briefly, a solution of 10 nm AuNPs were twice washed in a borate buffer solution at pH ~ 8. 450 μg of C225 with linker was slowly added to a 1000 μg AuNP solution. It was placed on a continuous mixer and incubated at room temperature for 4 hours. Next, the conjugate was concentrated 15-fold in a 50,000 molecular weight centrifugation filter unit (Millipore Corp., Billerica, MA) at 3,800 × g.

Since PAM4 does not have the same glycosolation status in the Fc region as C225, it was directly conjugated to slightly larger AuNPs without a linker via a thiol-gold interaction. First, PAM4 IgG was washed in borate buffer (pH ~ 8) twice and resuspended at a concentration of 2 mg/mL. A monovalent single molecule IgG (Fc + Fab with reactive sulfur groups on the heavy chain formerly of the disulfide bond) was created by reducing the interchain disulfide bond at the hinge region with 3 molar excess of tris (2-carboxyethyl) phosphine (TCEP). TCEP is a relatively gentle, but very specific, non-sulfur containing disulfide bond reducing agent that does not reduce heavy-light intrachain disulfide bonds or internal disulfide bonds at the antigen binding site at these concentrations (21). Subsequently, 450 μg of “activated” PAM4 was mixed with 1000 ug 20 nm AuNP in borate buffer and mixed for 4 hours in the dark at room temperature to permit the reduced sulfur moieties to directly form thiol-gold bonds on the AuNPs. The construct was twice washed with borate buffer, concentrated 15-fold in a 50,000 molecular weight centrifugation filter unit (Millipore Corp., Billerica, MA) at 3,800 × g.

A small shift in the peak plasmonic absorbance of the AuNPs (NS1, Applied NanoFluorescence, Houston, TX) was indicative of a non-aggregated conjugation state after challenge with equivolume 10% sodium chloride (21). Dynamic light scattering (DLS, Horiba, Ltd., Irvine, CA) determined the average hydrodynamic diameter of the constructs (500 measurements per sample in triplicate).

Target protein expression in Panc-1 and Capan-1 cells with immunoprecipitation

EGFR-1 and MUC-1 cell membrane expression was confirmed by Western blot analysis. Briefly, cell pellets were lysed with cold radioimmunoprecipitation assay (RIPA) buffer and centrifuged at 13,000 rpm for 30 minutes. The protein extracts (50 μg/lane) were electrophoresed on Bis-Tris protein gel, transferred to a PVDF membrane, and sequentially incubated in 5% dry milk and primary antibodies (BD Biosciences, Franklin Lakes, NJ and Immunomedics, Inc., Morris Plains, NJ). Next, the membranes were incubated with secondary antihuman IgG antibodies (H+L chains, Jackson ImmunoResearch, West Grove, PA). Images were acquired by a high-resolution photo scanner (CanoScan 4400F, Canon, Inc., Lake Success, NY) after the bands were detected with a peroxide solution (GenDEPOT, Inc., Barker, TX).

Confocal imaging of antibody conjugated AuNPs *in vitro*

Confocal images were prepared by growing Panc-1 cells on standard 1.5 glass cover slips which were treated with AlexaFluor (AF)-647 labeled C225 (the primary antibody delivered to living cells), 10 nm AuNP alone, the labeled C225-AuNP conjugated construct, or neither for 3 hours. Cell membranes were stained with 5 μg/mL wheat germ agglutinin conjugated to AF 594 (Invitrogen Corp., Carlsbad, CA) by incubating the cover slip for 10 minutes at 37°C. After PBS washings, the cells were fixed with 4% paraformaldehyde and permeabilized with cold 100% methanol. Blocking was performed for 1 hour with blocking solution (3% BSA + 1% animal serum in PBS). Cells were washed and stained with AF 488 labeled secondary antibody against the heavy and light chains of human IgG (Invitrogen Corp., Carlsbad, CA). After washing, DNA was stained with 4′, 6-diamidino-2-phenylindole dihydrochloride (DAPI, 300 nM) for 5 minutes. Cover slips were mounted (Dako Denmark A/S, Denmark), dried, sealed, and stored in the dark at 4°C until analyzed (Olympus DSU with Orca II ER camera, Olympus America Inc., Center Valley, PA).

In a separate experiment, Panc-1 cells were treated with AF 647 labeled C225 at the same concentration with or without AuNPs in order to determine the percent of cells *in vitro* with measurable amounts of primary fluorophore labeled C225-AuNP. Cells were identified in the usual manner by an automated cytometer while the fluorescence of AF 647 was simultaneously measured for individual cells (Cellometer Vision, Nexcelom Bioscience, LLC., Lawrence, MA). A fluorescence threshold of 7 arbitrary units was chosen to separate positive from negative populations based on the control sample. 1800 cells were counted for each group, and a histogram was created for each group with the same binning (Sigma Plot version 11, Systat Software Inc., San Jose, CA).

TEM imaging *in vitro*

Cell pellets were fixed with a 3% glutaraldehyde/2% paraformaldehyde solution in 0.1M cacodylate buffer at pH ~ 7.4. Samples were washed with 0.1% cacodylate buffered tannic acid, treated with 1% buffered osmium tetroxide, and stained with 1% uranyl acetate. The samples were ethanol dehydrated and embedded in LX-112 medium. After polymerization, the samples were cut with a Leica Ultracut microtome (Leica, Deerfield, IL), double stained with uranyl acetate/lead citrate in a Leica EM stainer, and imaged with a JEM 1010 TEM (JEOL, USA, Inc., Peabody, MA) at an accelerating voltage of 80 kV. Images were acquired with AMT Imaging System (Advanced Microscopy Techniques Corp., Danvers, MA).

Determination of gold concentration with inductively coupled plasma atomic emission spectrometry (ICP)

Cell pellets, tumor specimens, and organ specimens (liver, spleen, kidneys, and lung) were sectioned, weighed (cells were counted), and gently washed with PBS. Samples were partially digested with ~ 2 mL certified 30% H_2O_2 and evaporated. Next, 5 mL aqua regia (1 part nitric acid combined with 3 parts hydrochloric acid by volume, in a fume hood) was slowly added to each sample as the temperature was slowly raised to 130°C in order to completely digest the samples. After 3 hours, the samples were passively cooled and diluted with 18 Mω water to a final volume of 10 mL. The gold concentration of each sample was determined by ICP according to manufacturers' recommendations (iCAP 6500, Thermo Fisher Scientific, Walthorm, MA).

Nanoparticle heating in an RF field

Triplicate solutions of various concentrations of AuNPs alone or conjugated to antibodies were placed in the RF field in a transparent, 1.5 mL quartz cuvette directly on a copper ground plate and exposed to a high voltage RF field at 600W generator power for 1 minute

(13.56 MHz, 10 cm air gap, ThermMed, LLC, Inc., Erie, PA). Temperatures were recorded every 30 seconds with an infra-red camera (FLIR SC 6000, FLIR Systems, Inc., Boston, MA).

Panc-1 *in vitro* RF field exposure and cytotoxicity after C225-AuNP treatment

Panc-1 cells were plated in quadruplicate at a concentration of 1×10^6 cells/mL in 60mm dishes and incubated overnight. Negative controls remained untreated while the others were treated with C225 alone or C225-AuNP. Separate groups (n = 4 each) underwent RF field exposure at 600W for 10 minutes. Bulk media temperature remained between 36°C and 41°C as measured by an infra-red camera (FLIR SC 6000, FLIR Systems, Inc., Boston, MA). Viability was measured with flow cytometry (LSRII, BD Biosciences, Franklin, NJ) 36 hours after exposure. Briefly, cell media (i.e., dying cells that were floating) was collected and the adherent remaining cells were released with trypsin. The trypsin was then neutralized with cell media and the cells were collected. Each sample was washed and stained without fixation or permeabilization. After a final wash, 50,000 cellular events were acquired for each sample and analyzed with FlowJo 8.8.6 (TreeStar, Inc., Ashland, OR). After gating the single cell population, Annexin V, a protein that binds to membrane protein phosphatidylserine, positive cells were considered apoptotic while propidium iodide, a chemical that fluoresces when bound to DNA, positive cells were considered necrotic. Annexin V and PI double positive cells were considered dead cells while double negative cells were characterized as viable.

Panc-1 and Capan-1 pancreatic xenografts AuNP treatment and RF field exposure

Nude balb/c mice (NCI Mouse Repository, Frederick, MD) were subcutaneously injected with either 3×10^6 Panc-1 or Capan-1 cells to the right flank (n = 20 each cell line). After the tumors were palpable (approximately 3 weeks), mice within each cancer cell type were randomly assigned to 1 of 4 groups. The mice with Panc-1 xenografts were treated/exposed to no treatment, C225-AuNP without RF exposure, RF exposure alone, or C225-AuNP treatment plus RF exposure. The mice were treated with C225-AuNP 10 mg/kg by gold weight injected intraperitoneally (IP) to prevent AuNP collection at the site of an extremity (i.e., tail vein). RF exposure consisted of 600W generator power for 10 minutes with an air gap of 10 cm. All antibody-AuNP treatments occurred weekly while all RF exposures occurred ~36 hours after treatments on a weekly basis. Tumors were measured 48 hours after RF exposure each week while C225-AuNP treatment and RF exposure began after week 1.

Mice with Capan-1 tumors were randomly assigned to 1 of 4 groups as well (n = 5 each group). Those groups were untreated control, PAM4-AuNP treatment only, unconjugated AuNP treatment plus RF field exposure (600W generator power, 10 minute duration, air gap of 10 cm), and PAM4-AuNP treatment weekly with the same RF exposure weekly. Unconjugated AuNP and PAM4-AuNP were also treated IP at 10 mg/kg by gold weight for each.

During the experiment, all mice were kept in accordance with an Institutional Animal Care and Use Committee approved protocol. In order to safely expose the animals to RF fields, their tails, ears, and paws were completely grounded to avoid excess current in the extremities that would result in electrothermal injuries. This was accomplished by placing mice directly on a large grounded copper plate and attaching conducting copper tape (3M, St. Paul, MN) to the extremities and plate.

Mice were sedated with ketamine 0.1mg/g and xylazine 0.01 mg/g IP prior to each RF field exposure and monitored thereafter. The temperature of each mouse was continuously

measured with an infrared camera (FLIR SC 6000, FLIR Systems, Inc., Boston, MA), and at no time did their temperatures exceed 41.5°C. For the first minute of every RF field exposure, a cuvette with 100 μg/mL 20 nm AuNPs was placed within 1.5 cm of the tumor. This served as control to confirm heating of AuNPs in the RF field. After 1 minute, the RF field generator was briefly turned off (less than 2 seconds) to remove the cuvette, as it approached boiling temperatures soon thereafter.

Tumor volumes (width squared X length) were measured weekly with electronic calipers. After 6 weeks of treatment, the animals were euthanized and selected organs were harvested for gold biodistribution and histopathological evaluation (liver, spleen, kidney, lung, and tumor). For evaluation of normal organ and tumor-specific injury, specimens were prepared for histological procedures, embedded in paraffin, and sectioned at 5 μm. The sections were stained with hematoxylin and eosin stain (H&E) and examined by light microscopy. Injury was assessed by grade (Grade 1: rare, < 10%; Grade 2: mild, 10%–20%; Grade 3: moderate, 20–50%; Grade 4: severe, >50%) by an expert in comparative mammalian pathology (ANH).

Confocal immunofluorescent microscopy *in vivo*

Tumor sections on standard glass slides were deparaffinized by heating to 60°C for 1 hour. They were then de-waxed and rehydrated by sequential washing for ~ 5 minutes in xylene (×3) followed by decreasing concentrations of ethanol in water. Sections were then placed in boiling antigen retrieval buffer (citrate based, pH = 6, 0.5% Tween-20). This was heated in a microwave at boiling temperatures for an additional 1 minute. Next, the sections were microwaved in the buffer for 15 minutes at 30% power. Sections were then washed with PBS and placed in blocking solution for 1.5 hours (1% bovine serum albumin and 2% fetal bovine serum in PBS). Sections were stained with an antibody to cleaved caspase-3 (Cell Signaling Technology, Danvers, MA) diluted 1:250 in blocking solution for 1 hour at room temperature. Sections were thrice washed with PBS and a secondary antibody conjugated to Alexa Fluor 488 was applied to each (1:300) for 1 hour at room temperature. Sections were washed thrice in PBS, stained with DAPI (300 nM for 10 minutes), and a final washing in PBS. Fluorescent mounting media was applied (Dako North America, Inc., Carpinteria, CA) and the sections were sealed with a 1.5 cover slip.

Statistical Methods

Results are means ± standard errors of the mean unless otherwise noted. Statistical significance, α, was set to $p = 0.05$. Two-tailed Student's t-test compared differences in means between groups while multi-way analysis of variation analyzed tumor volumes (ANOVA, SPSS version 16.0, SPSS Inc., Chicago, IL). Data were plotted with Sigma Plot version 11 (Systat Software Inc., San Jose, CA).

Results

Characterization of antibody conjugated AuNPs

Directional conjugation of 10 nm AuNP to cetuximab via a covalent linker was confirmed by a small shift (< 10 nm) in peak plasmonic absorption (Figure 1). The small shift in the peak and similar width is consistent with AuNP conjugation and not consistent with AuNP aggregation (20). A PAM4 hemi-antibody (single heavy and light chain IgG with activated sulfur moieties) was conjugated to 20 nm AuNPs via a direct thiol-gold linkage and confirmed by a small shift in peak plasmonic absorption (Figure 1). The hydrodynamic diameter of C225-AuNP is 32.6 nm ± 0.7 nm while it is 36.9 nm ± 1.5 nm for PAM4-AuNP. Conjugated and unconjugated AuNPs heated in a concentration dependent fashion while the

C225-AuNP construct heated significantly faster in an RF field at 600W than unconjugated AuNPs (Figure 1D, $p < 0.0001$).

Time dependent internalization of C225 conjugated AuNPs to Panc-1 cells *in vitro*

Confocal microscopy demonstrated qualitatively different internalization rates after various treatment durations of C225-conjugated AuNPs compared to C225 alone (Figure 2). Briefly, the conjugation to gold produced punctate, spherical fluorescence initially along the cellular membrane which was then internalized into the cytoplasm (Figure 2, Supplemental Movie 1). This indirectly suggests that AuNP constructs are transported between cells (Supplemental Movie 1). C225 alone seems to have internalized faster than antibody-conjugated AuNPs. In a separate experiment, fluorescence from a fluorophore directly attached to C225 demonstrated significant overlap *in vitro* to secondary antibodies conjugated to a different fluorophore suggesting most of the primary antibody remains intact even after internalization (Figure 3). Nearly 90% of cells contain measurable C225-AuNPs based on direct fluorescence labeling (Figure 3, $p < 0.0001$ compared to background in untreated cells). In addition, after 3 hours of treatment, there were significantly more AuNPs delivered by C225 compared to unconjugated AuNPs (untargeted) *in vitro* (2.1 pg/cell ± 0.1 pg/cell vs. 0.2 pg/cell ± 0.1 pg/cell, respectively, $p = 0.005$).

Apoptosis mediated cell death after C225-AuNP treatment and RF exposure *in vitro*

C225 AuNPs (Figure 4A) induced significant cell death via apoptosis 36 hours after RF field exposure based on flow cytometric analysis ($p = 0.00005$ compared to untreated controls, Figure 4B). Neither C225 treatment alone (no AuNPs) with RF exposure nor C225-AuNP treatment alone without RF induced as much cell death as the combined treatment (Figure 4B).

Destruction of Panc-1 xenografts due to C225-AuNP treatments and RF exposure without injury to other organs

Excess electrical current on the surface of mice was grounded with copper conducting tape attached to the extremities in order to prevent non-specific electrothermal injuries (Figure 5A). While no mice developed electrothermal injuries during RF field treatment, AuNPs in adjacent quartz cuvettes continued to heat rapidly demonstrating the RF-induced thermal effect (Figure 5B, Supplemental Figure 1). Tumor temperatures in bulk rose above body temperatures by approximately 3°C during the first minute of RF exposure and remained stable thereafter (Figure 5B, Supplemental Figure 1).

Despite C225 conjugation, the biodistribution of AuNPs demonstrated increased concentration in the liver and spleen based on ICP analysis. Delivery of the C225-AuNP construct by intraperitoneal injection yielded tissue gold levels of 25.1 ± 6.4 mg AuNP/g tumor, 257.6 ± 7.5 mg AuNP/g spleen, 302.7 ± 82.5 mg AuNP/g liver, 4.0± 0.3 mg AuNP/g lung, and 4.1± 0.1 mg AuNP/g kidney. No murine tissues (liver, spleen, kidneys, and lung), demonstrated any evidence of acute or chronic injury based on histopathological analysis despite the presence of AuNPs.

Although Panc-1 control tumors had baseline evidence of central necrosis consistent with an aggressive carcinoma, the tumors from mice treated with C225-AuNP + RF field exposure demonstrated at least one grade increase in necrosis not seen in tumors from the other control groups (Figure 6A). Panc-1 tumors exposed to RF fields after C225-AuNP treatment were significantly smaller after 6 weeks than tumors treated with C225-AuNP alone ($p = 0.0097$, Figure 6B). In addition, cleaved caspase-3 was increased in Panc-1 tumors from mice treated with C225-AuNPs and exposed to the RF field compared to tumors from

control mice (Figure 6C and D). Tumor control was demonstrated after the first week of treatment (treatment began between weeks 1 and 2, overall $p = 0.004$, Figure 6E).

The mice exposed to RF fields (with or without C225-AuNP treatment) did not demonstrate any evidence of behavior changes, gross injuries, or other signs of treatment toxicity during the experiment. Importantly, sections of the lungs, spleen, kidneys, and liver did not demonstrate any evidence of acute or chronic injury on extensive histopathological exam despite the presence of AuNPs and RF field exposure (Figure 6, Supplemental Figure 2).

Destruction of Capan-1 human pancreatic xenografts after PAM4-AuNP treatment and RF field exposure

After demonstrating that C225-AuNP could effectively control pancreatic xenografts, we investigated this model further by utilizing a potentially more pancreatic cancer specific antibody, PAM4, and a unconjugated AuNP + RF control arm (Figure 6F). Capan-1 xenografts demonstrated statistically smaller tumors over the course of the experiment after PAM4-AuNP treatment and RF field exposure began between weeks 1 and 2 ($p = 0.035$, Figure 6F). Interestingly, the unconjugated AuNP + RF control arm (Figure 6F, blue line) demonstrated early effectiveness at decreasing tumor volumes that was lost by week 5. However, PAM4-AuNP treatment without RF exposure did not significantly reduce the size of Capan-1 tumors from the untreated controls (Figure 6). Similar to Panc-1 cancers, Capan-1 tumors treated with PAM4-conjugated AuNPs followed by RF field exposure were necrotic compared to control tumors treated with RF field exposure or PAM 4-targeted AuNPs alone (data not shown).

Again there was no evidence of injury to any of the selected organs (liver, spleen, kidneys, or lung) on histopathological analysis in the experimental groups. Furthermore, there were no changes to gross behaviors or habits of the animals throughout the course of the experiment.

Discussion

The obvious goal and major hurdle of cancer therapy is to kill cancer cells without injury to normal or bystander cells, tissues, or organs. We have demonstrated that RF fields can induce intracellular hyperthermic cytotoxicity with targeted gold nanoparticles while controlling relatively large pancreatic cancer xenografts. Importantly, this occurred without any evidence of injury to selected normal tissues (liver, spleen, lung, and kidney), changes in animal behavior, or unexplained animal death. It is imperative that the AuNP and antibody remain conjugated until intracellular delivery. We are very confident that our constructs remain conjugated until delivery because of the optical absorption after sodium chloride challenge (Figure 1), the diameters of the final constructs, and differences in immunofluorescence imaging.

RF field exposure in this situation was “whole body” exposure. A consequence of this exposure is that the certain portions of animals within the field are at different electrical potentials. Variations in electrical potentials results in electrical currents that can produce skin burns. Larger animals, however, have the body mass to absorb this “excess” current whereas smaller animals, i.e., rodents, may have regions of increased electrical current with subsequent thermal injury to the ears, paws, and tails. In order to prevent this, we electrically grounded the animals’ extremities to the grounded plate of the RF device in a similar fashion to grounding pads used clinically for surgical electrocautery. Fortunately, we found this to be very effective without decreasing the ability to destroy the tumor as the tumors were not directly isolated from the RF field. The bulk temperature of the tumors continued to rise (Supplemental Figure 1) above the body surface temperature, consistent with bulk thermal

transfer from intracellular AuNPs to cancer cells to surrounding tissues which was visualized on the infrared camera.

The *in vitro* experiments described herein were planned and performed with the restrictions of the *in vivo* experiment in place. For example, raising the animals' body temperatures above 41.5°C was presumed to be injurious to normal tissues. Therefore, the *in vitro* protocol was performed with these limitations. Likewise, we investigated early apoptosis at a single time point. Previous studies have demonstrated both apoptosis and necrosis at varying time points after RF field exposure depending on the construct involved and the RF field utilized (7,8,22). Finally, AuNPs of slightly different sizes were used to demonstrate the effect while keeping the final construct size similar.

Although C225 was predominately utilized in this series of experiments because of ease of conjugation, it may have increased amounts of adverse events due to high expression of EGFR on the skin and in bowel mucosa among other normal tissues (23,24). C225-conjugated AuNPs were more effective than PAM4-conjugated AuNPs in destroying targeted tumors, but C225 as a targeting agent may have more adverse clinical events because of enhanced AuNP uptake in nonmalignant tissues. PAM4 seems to be much more pancreatic cancer specific, and functions only as a pancreatic adenocarcinoma targeting antibody with no intrinsic cytotoxic or growth inhibition characteristic (18,25,26). Furthermore, even antibodies that fail as monotherapy for pancreatic cancer may be an effective tool to deliver AuNPs. We did not include C225 or PAM4 only control groups in our animal studies because PAM4 does not affect cell proliferation and C225 alone has not been active against pancreatic cancer cells in the current *in vitro* studies or previous *in vivo* work (8,25). Realistically, conjugating AuNPs to several different targeting molecules that attach to ligands differentially expressed in heterogeneous cancer cell populations will be a better approach; we are currently performing such studies *in vitro* and *in vivo*. Enhancing thermal sensitivity of cancer cells may be achieved by incorporating a third component, such as a toxin or cytotoxic drug, to the antibody-AuNP construct in order to potentiate the hyperthermic effect and impede cell repair mechanisms. In this case, the AuNP would act as scaffolding for one or more targeting proteins, therapeutic toxins or chemotherapeutics to potentiate thermal toxicity, and it would also be the agent to produce heat from RF field exposure.

An obvious challenge in utilizing this therapy is both the specificity of the targeting antibody as well as the non-specific internalization by the liver and spleen. We demonstrated that neither the lungs nor the kidneys internalized significant amounts of AuNPs. We theorize that since the kidney and lungs act as "filtering" organs in addition to their primary functions, the small size of the AuNP constructs utilized herein permit passage of these nanoparticles without accumulation, although the development of liver toxicity will need to be closely monitored in the future. However, as we have demonstrated here, there was no evidence of liver injury despite clear presence of AuNPs and RF field exposure. We suggest that the regenerative characteristics of the normal hepatocytes tolerate hyperthermic treatment more so than other tissues, including tumors (27,28). Furthermore, there is evidence that the majority of splenic and hepatic uptake of nanoparticles is by tissue macrophages without major induction of proinflammatory cytokines (29–31). Splenic macrophages or hepatic Kupffer cells that endocytose AuNPs may be affected by RF field treatments, but these cells are rapidly repopulated from circulating macrophage populations (32). Finally, there was no evidence of acute or chronic injury as the bulk temperatures in the liver likely remained relatively normal.

Future experiments with this modality include the development of an orthotopic model as well as the investigations of micrometastatic disease. We have demonstrated that antibody

delivered AuNPs induce significant tumor destruction in a murine model of pancreatic carcinoma after RF field exposure.

Translational Relevance

Nanoparticle mediated hyperthermic therapy offers a treatment that potentially will simultaneously have less side effects than systemic chemotherapy and a more direct action on pancreatic cancer cells. Gold colloids have a long history of minimal side effects while non-ionizing radiation is known to be safe. However, since gold nanoparticles heat in non-ionizing radiation, there is the potential to non-invasively target or direct the hyperthermic effect. Pancreatic cancer, one of the deadliest cancers, has multiple targeted therapies in development. As we have demonstrated here, the proper combination of a targeting antibody conjugated with gold nanoparticles results in effective tumor destruction with minimal toxicity.

Supplementary Material

Refer to Web version on PubMed Central for supplementary material.

Acknowledgments

The authors wish to acknowledge Kristine Ash and Yolanda Brittain from the Department of Surgical Oncology, The University of Texas M.D. Anderson Cancer Center, for administrative assistance. We also acknowledge the staff and animal care technologists of the Department of Veterinary Medicine and Surgery, specifically Maurice J Dufilho, IV. In addition, we acknowledge Dr. Jared K. Burks, of the Flow Cytometry and Cellular Imaging Core, at The University of Texas M.D. Anderson Cancer Center (NCI Core Grant CA16672), for assistance with confocal microscopy.

Financial support: This work was funded from the NIH (U54CA143837), NIH M. D Anderson Cancer Center Support Grant CA016672, and an unrestricted research grant from the Kanzius Research Foundation (SAC, Erie, PA). ESG is an NIH T32 research fellow (T32 CA09599).

References

1. Katz MH, Wang H, Fleming JB, et al. Long-term survival after multidisciplinary management of resected pancreatic adenocarcinoma. Ann Surg Oncol 2009;16:836–47. [PubMed: 19194760]
2. Abbott DE, Baker MS, Talamonti MS. Neoadjuvant therapy for pancreatic cancer: a current review. J Surg Oncol 2010;101:315–20. [PubMed: 20187063]
3. Tabernero J, Van Cutsem E, Diaz-Rubio E, et al. Phase II trial of cetuximab in combination with fluorouracil, leucovorin, and oxaliplatin in the first-line treatment of metastatic colorectal cancer. J Clin Oncol 2007;25:5225–32. [PubMed: 18024868]
4. Jemal A, Siegel R, Ward E, Hao Y, Xu J, Thun MJ. Cancer statistics, 2009. CA Cancer J Clin 2009;59:225–49. [PubMed: 19474385]
5. Hirsch LR, Stafford RJ, Bankson JA, et al. Nanoshell-mediated near-infrared thermal therapy of tumors under magnetic resonance guidance. Proceedings of the National Academy of Sciences of the United States of America 2003;100:13549–54. [PubMed: 14597719]
6. Wang ZY, Song J, Zhang DS. Nanosized As2O3/Fe2O3 complexes combined with magnetic fluid hyperthermia selectively target liver cancer cells. World J Gastroenterol 2009;15:2995–3002. [PubMed: 19554652]
7. Curley SA, Cherukuri P, Briggs K, et al. Noninvasive radiofrequency field-induced hyperthermic cytotoxicity in human cancer cells using cetuximab-targeted gold nanoparticles. J Exp Ther Oncol 2008;7:313–26. [PubMed: 19227011]
8. Glazer ES, Curley SA. Radiofrequency field-induced thermal cytotoxicity in cancer cells treated with fluorescent nanoparticles. Cancer 2010;116:3285–93. [PubMed: 20564640]

9. Cardinal J, Klune JR, Chory E, et al. Noninvasive radiofrequency ablation of cancer targeted by gold nanoparticles. Surgery 2008;144:125–32. [PubMed: 18656617]
10. Gannon CJ, Cherukuri P, Yakobson BI, et al. Carbon nanotube-enhanced thermal destruction of cancer cells in a noninvasive radiofrequency field. Cancer 2007;110:2654–65. [PubMed: 17960610]
11. Storm FK, Harrison WH, Elliott RS, Morton DL. Normal tissue and solid tumor effects of hyperthermia in animal models and clinical trials. Cancer Res 1979;39:2245–51. [PubMed: 445424]
12. Ito Y, Kennan RP, Watanabe E, Koizumi H. Assessment of heating effects in skin during continuous wave near infrared spectroscopy. J Biomed Opt 2000;5:383–90. [PubMed: 11092426]
13. Germer CT, Roggan A, Ritz JP, et al. Optical properties of native and coagulated human liver tissue and liver metastases in the near infrared range. Lasers Surg Med 1998;23:194–203. [PubMed: 9829430]
14. Woodburn KW, Fan Q, Kessel D, Luo Y, Young SW. Photodynamic therapy of B16F10 murine melanoma with lutetium texaphyrin. J Invest Dermatol 1998;110:746–51. [PubMed: 9579539]
15. Cherukuri P, Gannon CJ, Leeuw TK, et al. Mammalian pharmacokinetics of carbon nanotubes using intrinsic near-infrared fluorescence. Proc Natl Acad Sci U S A 2006;103:18882–6. [PubMed: 17135351]
16. Antonovych TT. Gold nephropathy. Ann Clin Lab Sci 1981;11:386–91. [PubMed: 7036839]
17. Cherukuri P, Glazer ES, Curley SA. Targeted hyperthermia using metal nanoparticles. Adv Drug Deliv Rev. 2009
18. Gold DV, Karanjawala Z, Modrak DE, Goldenberg DM, Hruban RH. PAM4-reactive MUC1 is a biomarker for early pancreatic adenocarcinoma. Clin Cancer Res 2007;13:7380–7. [PubMed: 18094420]
19. Decuzzi P, Ferrari M. The receptor-mediated endocytosis of nonspherical particles. Biophys J 2008;94:3790–7. [PubMed: 18234813]
20. Kumar S, Aaron J, Sokolov K. Directional conjugation of antibodies to nanoparticles for synthesis of multiplexed optical contrast agents with both delivery and targeting moieties. Nat Protoc 2008;3:314–20. [PubMed: 18274533]
21. Hermanson, G. Bioconjugate Techniques. Vol. 2008. Academic Press; San Francisco: 2008.
22. Gannon CJ, Patra CR, Bhattacharya R, Mukherjee P, Curley SA. Intracellular gold nanoparticles enhance non-invasive radiofrequency thermal destruction of human gastrointestinal cancer cells. J Nanobiotechnology 2008;6:2. [PubMed: 18234109]
23. Sargent ER, Gomella LG, Belldegrun A, Linehan WM, Kasid A. Epidermal growth factor receptor gene expression in normal human kidney and renal cell carcinoma. J Urol 1989;142:1364–8. [PubMed: 2810532]
24. Koretz K, Schlag P, Moller P. Expression of epidermal growth factor receptor in normal colorectal mucosa, adenoma, and carcinoma. Virchows Arch A Pathol Anat Histopathol 1990;416:343–9. [PubMed: 2106751]
25. Gold DV, Goldenberg DM, Karacay H, et al. A novel bispecific, trivalent antibody construct for targeting pancreatic carcinoma. Cancer Res 2008;68:4819–26. [PubMed: 18559529]
26. Gold DV, Schutsky K, Modrak D, Cardillo TM. Low-dose radioimmunotherapy ((90)Y-PAM4) combined with gemcitabine for the treatment of experimental pancreatic cancer. Clin Cancer Res 2003;9:3929S–37S. [PubMed: 14506191]
27. Fausto N, Campbell JS, Riehle KJ. Liver regeneration. Hepatology 2006;43:S45–53. [PubMed: 16447274]
28. Du SS, Zeng ZC, Tang ZY, et al. Regenerative capacity of normal and irradiated liver following partial hepatectomy in rats. Int J Radiat Biol 2009;85:1114–25. [PubMed: 19995237]
29. Shukla R, Bansal V, Chaudhary M, Basu A, Bhonde RR, Sastry M. Biocompatibility of gold nanoparticles and their endocytotic fate inside the cellular compartment: a microscopic overview. Langmuir 2005;21:10644–54. [PubMed: 16262332]
30. Yen HJ, Hsu SH, Tsai CL. Cytotoxicity and immunological response of gold and silver nanoparticles of different sizes. Small 2009;5:1553–61. [PubMed: 19326357]

31. Cho WS, Cho M, Jeong J, et al. Size-dependent tissue kinetics of PEG-coated gold nanoparticles. Toxicol Appl Pharmacol 245:116–23. [PubMed: 20193702]

32. Yamamoto T, Naito M, Moriyama H, et al. Repopulation of murine Kupffer cells after intravenous administration of liposome-encapsulated dichloromethylene diphosphonate. Am J Pathol 1996;149:1271–86. [PubMed: 8863675]

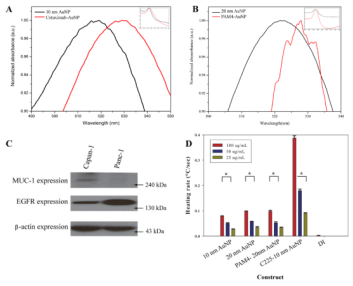

Figure 1.

Conjugation of 10 nm AuNP to cetuximab (C225) via a covalent linker (A) and 20 nm AuNP conjugated to PAM4 single chain IgG via thiol-gold interaction (B) was seen with appropriate shifts in the peak plasmonic absorbance after NaCl challenge. (C) Panc-1 expresses EGFR, the target of C225, while Capan-1 expresses the target of PAM4, MUC-1. Unconjugated and conjugated AuNPs in deionized water (DI) heat in the RF field in a concentration dependent manner (D, * $p < 0.0001$ between low and high concentrations).

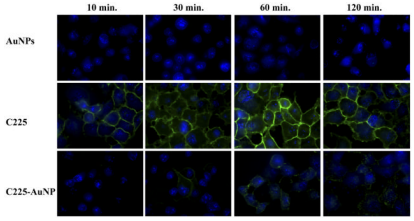

Figure 2.

C225 seems to quickly and uniformly binds to the surface of Panc-1 cells after treatment (durations listed at the top of each column) while C225-AuNP binds more slowly and in discrete, punctuate morphology consistent with an antibody conjugated to AuNPs. *Blue: DAPI bound to DNA. Green: AlexaFluor 488 labeled secondary antibody against human IgG.*

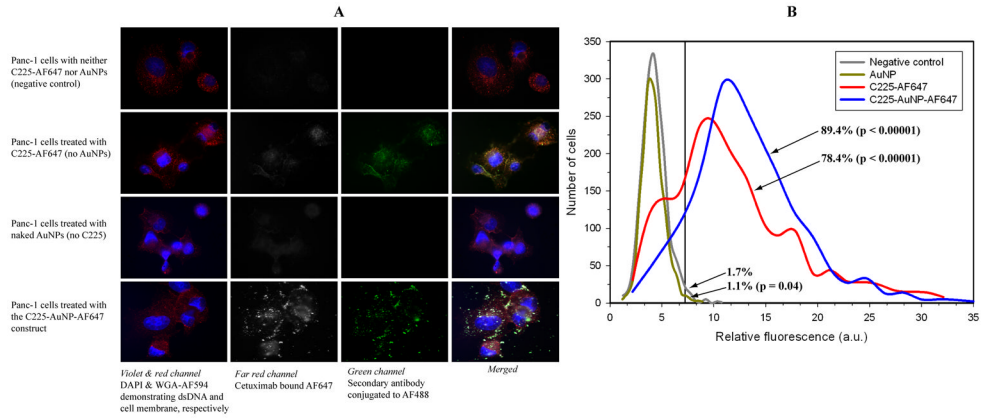

Figure 3.

AlexaFluor 647-labeled C225 demonstrates significant co-localization with the secondary anti-IgG suggesting that the C225-AuNP construct remains intact after internalization into the cell (A). Although there is mild autofluorescence (< 2%) in the far red channel (second column from left, confocal microscopy), using a fluorescent threshold of 7 arbitrary units (a.u.) demonstrates that over 78% of cells contain measurable levels of AF 647 labeled C225 regardless if AuNPs are conjugated (B, based on fluorescence cell counting). Percentages represent the proportion of cells with fluorescence greater than 7 a.u. while the p value compares the mean fluorescence intensity of each distribution to the negative control.

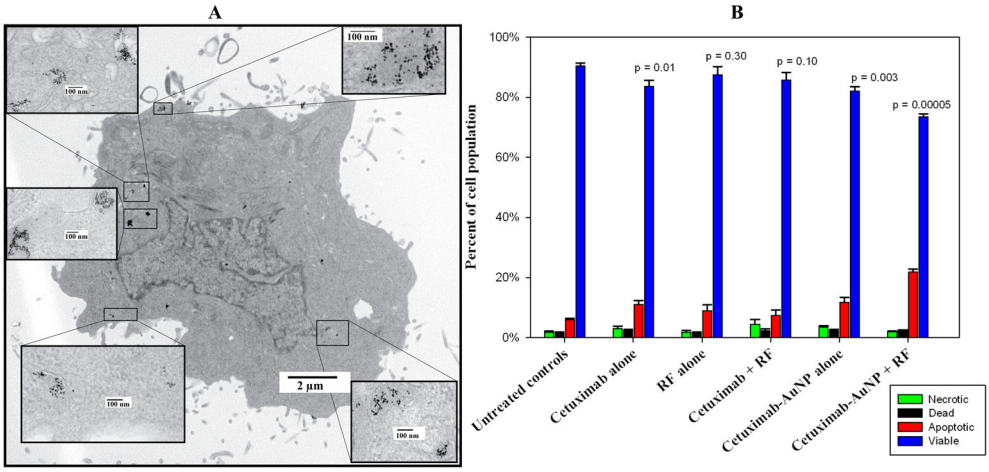

Figure 4.

TEM demonstrates internalization of AuNPs in Panc-1 cells after treatment with 100 μg/mL AuNP conjugated C225 for 3 hours (A). After RF field exposure, Panc-1 cells treated with C225-AuNP demonstrate significantly increased apoptosis (B, red bar). Statistical significance compares differences in the viable cell population (blue bar) between each group and the untreated control group based on flow cytometry (B, far left group).

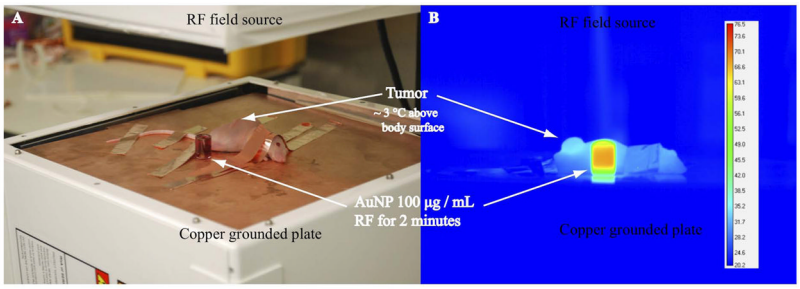

Figure 5.

Nude balb/c mice with pancreatic xenografts in the right flank were sedated and grounded to a copper plate with conducting copper tape in order to prevent excess current inducing electrothermal injury (A). Tumors heat significantly more so than the mouse body due to C225 mediated AuNP delivery (B). In addition, 100 µg/mL AuNPs in deionized water heat in an RF field whereas the conducting copper tape protects mice extremities (ears, tails, paws) from excess current and electrothermal injury.

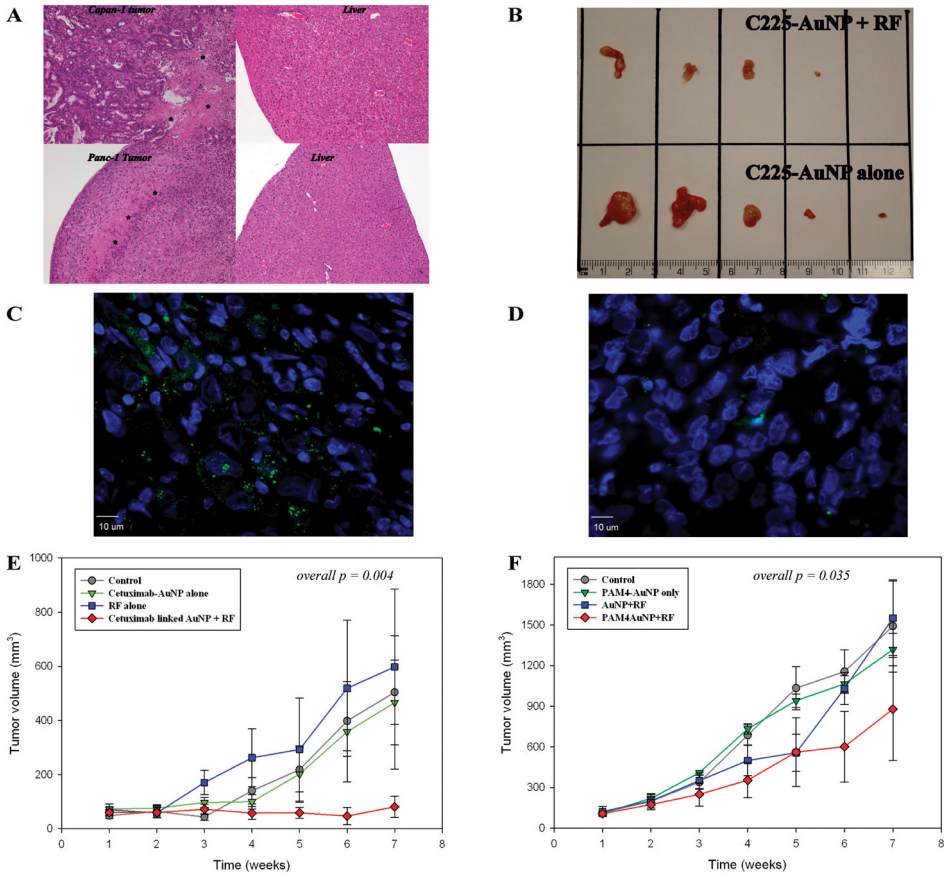

Figure 6.

Panc-1 and Capan-1 tumors demonstrated significant increases in necrosis (*) after treatment with antibody conjugated AuNPs and RF field exposure whereas liver tissue remained normal (A). Panc-1 tumors after 6 weeks of combined C225-AuNP treatment and RF exposure (B, top row) are significantly smaller than tumors in mice that just received C225-AuNPs treatment (p = 0.0097, B, bottom row). There was one complete response and one near complete response in the dual treatment group. Cleaved caspase-3 was increased in tumors from mice that had undergone antibody targeted gold nanoparticle treatment and RF field exposure (C, Panc-1 xenograft with DAPI in blue and cleaved caspase-3 labeled in green) compared to tumors from control mice (D, represented by the Panc-1 xenografts from untreated controls). RF exposure after antibody AuNP treatment resulted in significant decreased tumor volumes (E &F)